CHARACTERIZATION OF THE PANORAMIC ANNULAR LENS

David L. Lehner
Optical Fabrication Branch
George C. Marshall Space Flight Center
Marshall Space Flight Center, Alabama 35812

Donald R. Matthys
Physics Department
Marquette University
Milwaukee, Wisconsin 53233

Andrew G. Richter
Physics Department
Northwestern University
Evanston, Illinois, 60208

John A. Gilbert
Department of Mechanical and Aerospace Engineering
University of Alabama in Huntsville
Huntsville, Alabama 35899

ABSTRACT

The *Panoramic Annular Lens* (PAL) consists of a single piece of glass with spherical surfaces that produces a flat annular image of the entire 360 degree surround of the optical axis of the lens. An annular-shaped image of the surroundings of the lens can be imaged onto a film or sensor by the use of a transfer lens. When coupled with standard optical techniques, the unique imaging characteristics of the PAL provide powerful new tools for experimental stress analysis.

This paper describes the attributes of the PAL and presents an analytical formulation which shows that the PAL maps elements from object to image space via a constant aspect ratio polar mapping. These arguments are verified, first, by comparing the results obtained from the analytical formulation to images recorded through a PAL imaging system. Then, the results are compared with the mapping function established by using a ray tracing program written specifically to accommodate the PAL's unique geometry. The results obtained from these different formulations agree to within two percent.

1 INTRODUCTION

Inspection and measurement inside cylindrical cavities requires capturing a large field of view and presenting information in a fashion suitable for analysis. Attempts to produce optical systems capable of viewing continuous field panoramic images have been attempted many times, and were first patented in the 1880s [1]. Most panoramic imaging systems have met with limited success. Simpler systems with fewer optical elements tend to give discontinuous images, containing breaks or overlaps in the image [2], and more complex systems tend to be large and cumbersome, consisting of numerous optics and mirrors [3]. The *Panoramic Annular Lens* (PAL), however, provides an excellent solution to many of the problems associated with panoramic imaging [4].

As shown in Figure 1, the PAL is a single element imaging block comprised of three spherical optical surfaces, and one flat optical surface. Two of the spherical surfaces, shown as heavier lines on the figure, are mirrored while the third spherical surface and the flat surface are not. Rays leaving points A and B are refracted upon contacting the first spherical surface, and reflect off the rear mirrored spherical surface. They travel forward in the lens and strike the front mirrored spherical surface. Reflected back, the rays are refracted at the rear flat optical surface and diverge as they exit the lens. The divergent rays leaving the flat optical surface at the back of the PAL can be "back traced" to form virtual images corresponding to points A and B at the points labeled A' and B'. A biconvex lens, labeled as the collector lens, forms real images of these internal points at A" and B". Imaging all points contained within the field of view produces a flat annular image.

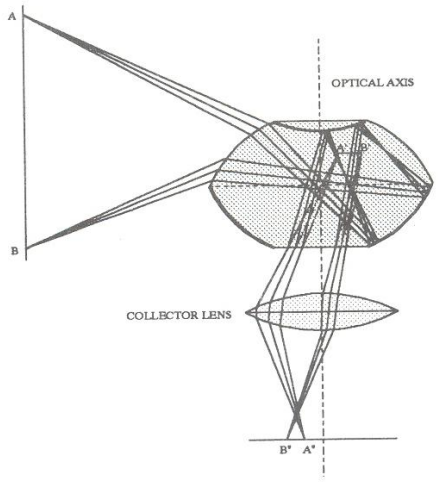

Fig. 1 Panoramic annular lens system.

The PAL has been used extensively for making inspections and measurements within cylindrical cavities and pipes. The associated applications, collectively referred to as radial metrology, either rely on visual inspection [5-7], structured light [8-11], holographic displacement analysis [12,13], time-average modal analysis [14], speckle metrology [15-17], or moire techniques [18]. Besides these applications in radial metrology, the PAL has been suggested as part of the guidance system for a ballistic missile [19], to capture panoramic images during spacecraft docking [20] and as a horizon sensor in a tethered satellite [21]. Work has also been performed to linearize the annular images to facilitate human viewing [22-24].

In all these studies, attempts to quantitatively analyze and linearize PAL images have relied on the experimental determination of the mapping characteristics from object to image space; an analytical representation has not yet been established. In the case of radial metrology, the lack of this knowledge makes it difficult to quantify *a priori* how much information can be obtained from a given cavity and the accuracy to which that information can be determined. It is also difficult to make meaningful comparisons between the PAL and more conventional lenses. These comparisons could be very important since they would help researchers to select the best imaging system for a given application.

This paper describes the attributes of the PAL and presents an analytical formulation which shows that the PAL maps elements from object to image space via a constant aspect ratio polar mapping. The results of the analysis are compared to those obtained from experimental data, and from the method of ray tracing.

2 The PANORAMIC ANNULAR LENS (PAL)

Further discussion of the PAL is simplified by establishing the coordinate system shown in Figure 2.

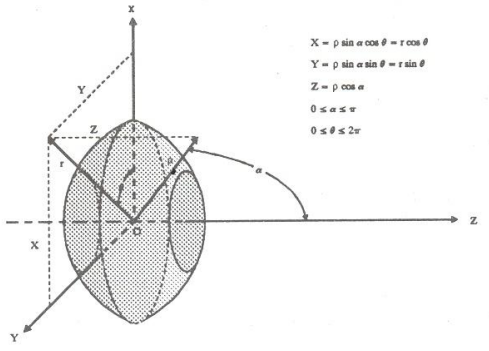

Fig. 2 Coordinate system and spherical coordinates used for radial metrology with a PAL.

The optical axis of the lens is defined by a line perpendicular to the flat surface which passes through the centers of curvature of the three spherical surfaces. A longitudinal axis, labeled Z, is chosen to coincide with the optical axis. Two other axes, labeled X and Y, are established in a plane defined by the physical equator of the lens. They are chosen to form a right handed triad with the longitudinal axis. Spherical coordinates (ρ,α,θ) may also be defined with respect to the origin.

In Figure 2, the angles α and θ are called the field angle and the radial position angle, respectively. The field angles corresponding to the points labeled A and B in Figure 1 are approximately 65° and 110°, respectively. They define the limits on the field of view for a 38mm (1.496in) diameter PAL made from Schott SF14 glass (n=1.76) and are referred to as the upper and lower field angles, respectively.

When the area between the upper and lower field angles is rotated around the optical axis through a radial position angle of 2π, a cylinder is described. This is illustrated in Figure 3 which shows the PAL and its continuous field of view. A collector lens is shown in the figure along with the annular image mapped by the collector lens into the flat image plane. The viewing of three dimensional cylindrical space as two dimensional flat space is referred to as flat cylindrical perspective [5].

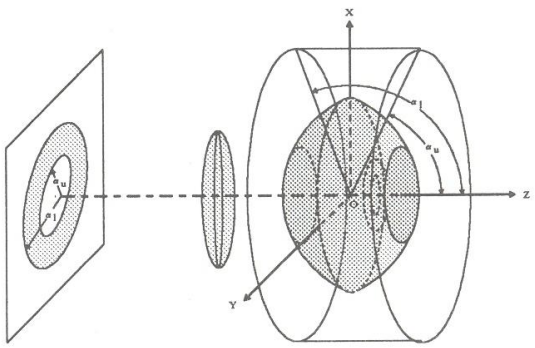

Fig. 3 Panoramic annular lens and its field of view.

The upper and lower field angles are a function of the index of the glass used in the PAL, with higher index glasses giving larger values for both. By changing the index of refraction, the field of view may be adjusted. This is an important consideration for radial metrology, since a better perspective of the cavity is obtained when the field of view subtends the equatorial plane.

3 CONVENTIONAL POLAR MAPPING

The PAL is designed to map a cylindrical field of view onto a flat image plane as a ring shaped annulus as opposed to a conventional lens which is designed to map a flat plane perpendicular to its optical axis to the image plane. When a conventional lens is used for radial metrology, a cylinder, whose inside surface is composed

of a uniform grid of squares, is mapped into the image plane as a series of evenly spaced concentric rings representing equally spaced lines drawn around the circumference of the cylinder; radial lines represent the longitudinal lines drawn along the length of the cylinder at constant circumferential positions [25]. Figure 4, for example, shows a conventional polar map of a cylinder divided into twenty four squares around its circumference and twelve squares along its length. It can be seen in the figure that the polar segments representing the squares vary in shape as well as size radially in the image. Segments toward the center of the image are longer in the radial direction than in the circumferential direction; whereas, segments toward the outer edge of the image are considerably longer in the circumferential direction than they are in the radial direction. Only a few elements appear to have the same height and width.

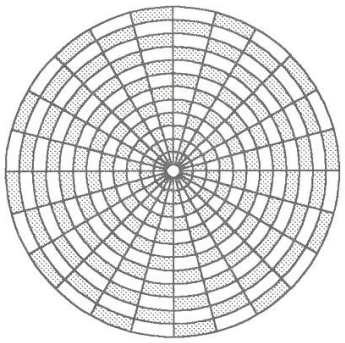

Fig. 4 A conventional polar map is recorded when a conventional 35mm lens is used to photograph a square grid wrapped around the inside wall of a cylinder.

Since the direction of "height" and "width" are somewhat arbitrary for radial metrology, they must be defined. In real (or object) space, height is measured as a longitudinal distance relative to the optical axis of a lens; width corresponds to a circumferential distance measured around the axis of the lens. In image space, height is measured as a radial distance relative to the center of an image; width corresponds to a circumferential distance measured around the image center. Once these parameters are established, it is possible to compute a real space as well as an image plane aspect ratio, defined as the height of the area divided by its width.

Figure 4 illustrates that, in the case of the conventional lens, square elements having a real space aspect ratio of unity are mapped to an image comprised of segments which have different image plane aspect ratios. As opposed to this polar map generated by a conventional lens, it will be demonstrated in the following section that a PAL maps the same uniform grid of squares into elements having constant image plane (polar) aspect ratios.

4 CONSTANT ASPECT RATIO POLAR MAPPING

Figure 5 shows a polar segment extracted from a polar mapping.

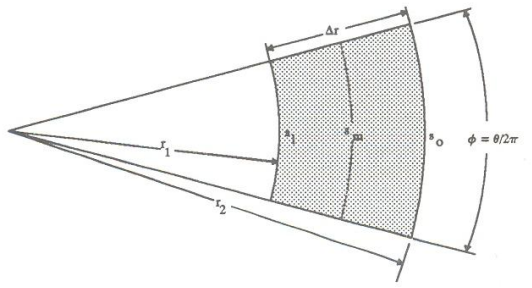

Fig. 5 A typical segment generated from a polar map.

The area of a polar section shown in Figure 5 can be written as:

$$\text{AREA} = (\pi r_o^2 - \pi r_i^2)\phi \tag{1}$$

where ϕ is the fraction of a circle subtended, and is dimensionless. Factoring Equation 1:

$$(\pi r_o^2 - \pi r_i^2)\phi = \pi\phi(r_o^2 - r_i^2) = \pi\phi(r_o - r_i)(r_o + r_i) \ . \tag{2}$$

It can be seen in the figure that $(r_o - r_i)$ is equal to the radial height, Δr, of the section. The arc lengths s_o and s_i can be written as the product of their respective radial distances r_o and r_i and θ, the angle they subtend measured in radians. Therefore, the term $(r_o + r_i)$ can be written as the sum of the arc lengths of the inside and outside edges of the element divided by θ. The angle ϕ is equivalent to θ divided by 2π. Finally, the sum of the arc lengths of the inside and outside edges of the element divided by two is equal to the arc length, (s_m), at the midpoint of the radial height of the element. These observations allow Equation 2 to be rewritten as:

$$\begin{aligned} \pi\phi(r_o^2 - r_i^2) &= \pi\phi(\Delta r)\left(\frac{s_o + s_i}{\theta}\right) \\ &= \left(\frac{\theta}{2}\right)(\Delta r)\left(\frac{s_o + s_i}{\theta}\right) = (\Delta r)\left(\frac{s_o + s_i}{2}\right) \\ &= (\Delta r)s_m \ . \end{aligned} \tag{3}$$

The above equation shows that the area of a polar segment is equal to the radial height times the midpoint arc length. Thus the area and aspect ratio for a polar type segment are given by

$$A \equiv \text{AREA} = \Delta r \; s_m$$

$$\kappa \equiv \text{ASPECT RATIO (POLAR SEGMENT)} = \frac{\Delta r}{s_m} \; . \tag{4}$$

A polar map consisting of elements having constant polar aspect ratios can be constructed by considering Figure 6 which shows two consecutive segments in the image plane.

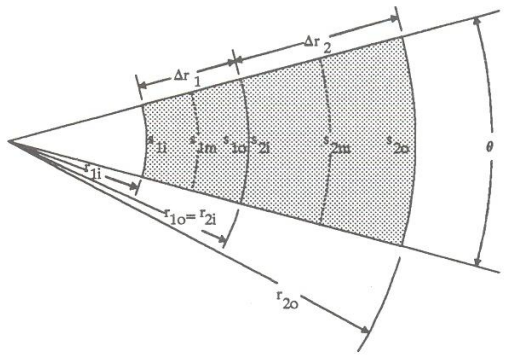

Fig. 6 Consecutive constant aspect ratio polar segments.

For these segments to subtend the same angle, the outside arc length of the inner element must be equal to the inside arc length of the outer element. Assuming the aspect ratios of the two elements to be equal:

$$\frac{\Delta r_1}{s_{1m}} = \frac{\Delta r_2}{s_{2m}} = \kappa \; . \tag{5}$$

Rewriting in terms of the inner and outer radius arc lengths:

$$\frac{r_{1o}-r_{1i}}{\left(\frac{s_{1o}+s_{1i}}{2}\right)} = \frac{r_{2o}-r_{2i}}{\left(\frac{s_{2o}+s_{2i}}{2}\right)} \; . \tag{6}$$

Writing the arc lengths as functions of radii drawn from the image center:

$$\frac{r_{1o}-r_{1i}}{\theta\left(\frac{r_{1o}+r_{1i}}{2}\right)} = \frac{r_{2o}-r_{2i}}{\theta\left(\frac{r_{2o}+r_{2i}}{2}\right)} \; . \tag{7}$$

Multiplying both sides by θ/2:

$$\frac{r_{1o}-r_{1i}}{r_{1o}+r_{1i}} = \frac{r_{2o}-r_{2i}}{r_{2o}+r_{2i}} \tag{8}$$

cross multiplying:

$$(r_{1o}-r_{1i})(r_{2o}+r_{2i}) = (r_{2o}-r_{2i})(r_{1o}+r_{1i}) \tag{9}$$

expanding:

$$r_{1o}r_{2o}+r_{1o}r_{2i}-r_{1i}r_{2o}-r_{1i}r_{2i} = r_{2o}r_{1o}+r_{2o}r_{1i}-r_{2i}r_{1o}-r_{2i}r_{1i} \tag{10}$$

and simplifying:

$$2r_{1o}r_{2i} = 2r_{1i}r_{2o} \; . \tag{11}$$

This result can be rearranged to show that the ratio of the inner and outer boundary radii of each polar segment is constant for constant aspect ratio segments. That is:

$$\frac{r_{1i}}{r_{1o}} = \frac{r_{2i}}{r_{2o}} = \frac{r_{1o}}{r_{2o}} \; . \tag{12}$$

The above result can be used to determine the radial dimensions of subsequent polar segments once an initial segment has been established. The circumferential arc length of a polar element increases with increasing radial distance from the center of the map; consequently, the respective areas of sequential polar elements are different even when the aspect ratio of the elements remain constant.

An initial segment can be determined by picking a radial distance on the map, and calculating the arc length subtended for a specific angle θ. Using this distance as the midpoint arc length for the segment, the following relationship can be written:

$$s_m = r_m\theta = \frac{\theta(r_i+r_o)}{2} \; . \tag{13}$$

To retain constant perspective, the midpoint arc length must also be equal to the radial height of the element divided by the aspect ratio, which in equation form is:

$$s_m = r_m\theta = \frac{\Delta r}{\kappa} = \frac{r_o-r_i}{\kappa} \; . \tag{14}$$

Equating the right hand sides of Equations 13 and 14:

$$\theta\left(\frac{r_i+r_o}{2}\right) = \frac{r_o-r_i}{\kappa} \tag{15}$$

and solving for r_o:

$$r_o = r_i\left(\frac{2+\kappa\theta}{2-\kappa\theta}\right) \; . \tag{16}$$

Substituting the latter into Equation 15:

$$r_m\theta = r_o - r_i = r_i\left(\frac{2+\kappa\theta}{2-\kappa\theta}\right) - r_i = r_i\left(\frac{2\kappa\theta}{2-\kappa\theta}\right). \quad (17)$$

Finally, solving Equation 17 for r_i in terms of r_m:

$$r_i = r_m\left(\frac{2-\kappa\theta}{2}\right). \quad (18)$$

The expression for r_o can be derived in the same fashion, and is:

$$r_o = r_m\left(\frac{2+\kappa\theta}{2}\right). \quad (19)$$

Now that r_o and r_i have been established for one element, subsequent elements can be determined using the ratio of r_i and r_o, in Equation 12, as follows:

$$\frac{r_i}{r_o} = \frac{r_o}{r_?} \quad (20)$$

where $r_?$ is the outside radius of the next constant aspect ratio polar segment away from the center of the map. An alternative expression is:

$$\frac{r_i}{r_o} = \frac{r_?}{r_i} \quad (21)$$

in which case $r_?$ is the inside radius of the next constant aspect ratio polar segment towards the center of the map.

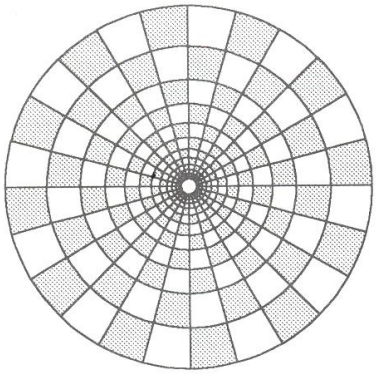

Fig. 7 A constant aspect ratio polar map is recorded when a PAL is used to photograph a square grid wrapped around the inside wall of a cylinder.

The above procedure was followed to generate Figure 7 which corresponds to a constant aspect ratio (with $\kappa = 1$) polar map for a cylinder with twenty four divisions around the circumference (15° increments), and twelve units of longitudinal length.

5 RELATIONSHIP BETWEEN OBJECT AND IMAGE SPACE

When a constant aspect ratio polar map is obtained in radial metrology, it is essential that the positions of points located in real space can be related to those in the image plane. To this end, consider the cylinder and the coordinate system shown in Figure 8.

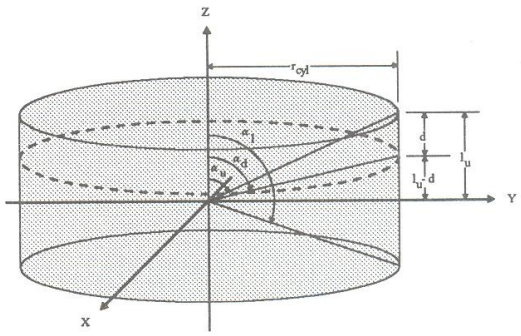

Fig. 8 Coordinate system axes and angles.

The axis collinear with the axis of the cylinder is labeled Z, and the orthogonal radial axes are labeled X and Y, respectively. The assumption is made that the upper edge of the cylinder is mapped to the inside radius of the polar map. The size of the radius chosen in the image plane defines the scaling factor for a geometrical construction and, in an actual PAL system, is determined by the magnification of the collector lens. The distance, d, measured from the upper edge of the cylinder to a given point located on the wall, is equivalent to a circumferential arc length which may be computed using:

$$d = r_{cyl}\theta \quad (22)$$

where r_{cyl} is the radius of the cylinder. The corresponding radius on the polar map is obtained by solving Equation 22 for θ, and substituting into Equation 16, which gives:

$$r_d = r_i\left(\frac{2r_{cyl}+\kappa d}{2r_{cyl}-\kappa d}\right). \quad (23)$$

In practice, knowledge of the angular position with respect to the coordinate system provides important information even when the absolute dimensions of the cylinder are not known *a priori*. This knowledge can be obtained by considering Figure 8 in which lines

drawn from the origin to the upper and lower edges of the cylinder make angles of α_u and α_l, respectively, with the positive Z axis. The angle formed by a line drawn from the origin to a point located at a distance, d, below the upper edge of the cylinder is α_d.

The angle α_u can be written in terms of the distance from the origin to the top of the cylinder as follows:

$$\cot(\alpha_u) = \frac{l_u}{r_{cyl}} . \tag{24}$$

Angle α_d can be expressed in a similar fashion as:

$$\cot(\alpha_d) = \frac{l_u - d}{r_{cyl}} = \frac{l_u}{r_{cyl}} - \frac{d}{r_{cyl}} . \tag{25}$$

Substituting Equation 24 into Equation 25 and solving for d/r_{cyl}:

$$\frac{d}{r_{cyl}} = \cot(\alpha_u) - \cot(\alpha_d) . \tag{26}$$

Solving Equation 23 for d/r_{cyl}:

$$\frac{d}{r_{cyl}} = \frac{2}{\kappa}\left(\frac{r_d - r_i}{r_d + r_i}\right) . \tag{27}$$

Setting the right hand sides of Equations 26 and 27 equal, and solving for $\cot(\alpha_d)$:

$$\cot(\alpha_d) = \cot(\alpha_u) - \frac{2}{\kappa}\left(\frac{r_d - r_i}{r_d + r_i}\right) . \tag{28}$$

Finally, solving Equation 28 for α_d:

$$\alpha_d = \tan^{-1}\left(\frac{\kappa(r_d + r_i)\tan(\alpha_u)}{\kappa(r_d + r_i) - 2(r_d - r_i)\tan(\alpha_u)}\right) . \tag{29}$$

Equation 29 shows that when the angle from the origin to the upper edge of a cylinder is known in real space, the angle from the origin to any point can be determined from measurements taken in the image plane.

6 VERIFICATION OF THE MAPPING CHARACTERISTIC

An experimental procedure to determine the parameters necessary to compare the results predicted by the above equations with a photograph actually taken through the PAL was recently reported [26]. The PAL was mounted in a vertical position on a CCD video imaging system with a resolution of 512 by 512 pixels. Three vertical target boards were placed a constant distance from the optical axis of the lens at 120° spacings; this configuration ensured that the PAL was aligned with the targets. Marks were placed on the targets corresponding to the lowest and highest points which could be seen in the PAL image. The angles which the marks on the target made with respect to the optical axis of the lens were then calculated. Upper and lower field angles of 64° and 107.7° were obtained.

During these tests, the radii of the inside and outside edges of the annular image were found to be 100 and 188 pixels, respectively. Equation 28 can be rewritten to solve for the aspect ratio of the image (with r_o and α_o substituted for r_d and α_d) as follows:

$$\kappa = \left(\frac{2}{\cot(\alpha_u) - \cot(\alpha_o)}\right)\left(\frac{r_o - r_i}{r_o + r_i}\right) . \tag{30}$$

An aspect ratio of 0.7574 is obtained when the values reported are substituted into this equation.

The first step in generating the polar map is to arbitrarily choose a value for the outer radius of the annular image. Then Equation 27 is rearranged to solve for the inside radius of the map as follows:

$$r_i = r_o\left(\frac{2 - \kappa(\cot(\alpha_u) - \cot(\alpha_o))}{2 + \kappa(\cot(\alpha_u) - \cot(\alpha_o))}\right) . \tag{31}$$

Assuming that r_o = 6.99cm (2.75in) and using κ=0.7574, α_u=64°, α_o=107.7°, Equation 31 gives a value r_i = 3.72cm (1.463in). Equation 31 can be rearranged once more to establish the radial distances corresponding to the 15° grid squares as follows:

$$r_d = r_i\left(\frac{2 + \kappa(\cot(\alpha_u) - \cot(\alpha_o))}{2 - \kappa(\cot(\alpha_u) - \cot(\alpha_o))}\right) . \tag{32}$$

The map shown in the lower half of Figure 9 was obtained using Equation 32 and reducing the field angle from 107.7° in 15° increments. The upper half of the figure shows a photograph taken through the PAL of a 15° grid of white and black squares placed in an actual cylinder.

An alternate method of verifying that the PAL produces a constant aspect ratio polar map is to compare the results obtained above with those obtained by ray tracing. In [26], the PAL was modeled with a ray tracing program written specifically to accommodate the lens' unique geometry. Rays were traced from an imaginary cylinder through an analytical lens model, and the locations of the focus of groups of rays were plotted. The distance to various points of focus from the inside radius of the annular image was determined by the location from which rays originated on the

imaginary cylinder. By plotting numerous rays from different positions on the imaginary cylinder and their respective focal point locations, a graph showing the theoretical mapping function of the lens was generated. A third order curve was fit to the data; the mapping (or "linearization") function obtained was:

$$\text{Image Height} = 0.1011\left(\frac{d}{r_{cyl}}\right)+0.0691\left(\frac{d}{r_{cyl}}\right)^2+0.0084\left(\frac{d}{r_{cyl}}\right)^3 \quad (33)$$

In this case, the value of the distance measured from the highest visible edge of the cylinder to the point in question divided by the radius of the cylinder, d/r_{cyl}, ranged from 0 to 0.95; the image height was measured from the inside radius of the image outward.

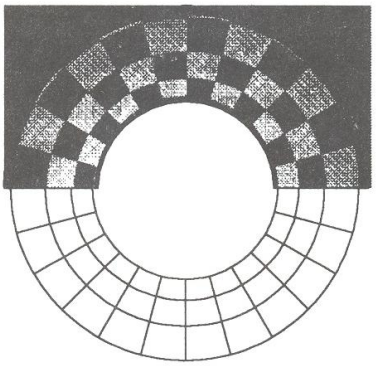

Fig. 9 A comparison of the analytical polar map to a photograph of a square grid taken through a PAL.

A comparison can be made with the constant aspect ratio polar mapping equations developed earlier using Equation 24 twice: first to establish the aspect ratio for the map, and then to describe a continuous mapping function. The inside radius of the image, r_i, was reported [26] to be equal to 0.13738 in. The outside image radius, r_o, is found by adding the inside radius to the image height predicted by Equation 33 at $\{d/r_{cyl}\}_{max}$, as 0.30299 in. Solving Equation 27 for κ, substituting the outside radius of the image for r_d, and using $\{d/r_{cyl}\}_{max}$ gives the following expression for the aspect ratio:

$$\kappa = 2\left(\frac{r_o-r_i}{r_o+r_i}\right)\left(\frac{r_{cyl}}{d}\right)_{max} \quad (34)$$

Substituting known values, $\kappa = 0.79173$.

Solving Equation 27 for r_d gives an expression for the radial position of any point in the constant aspect ratio polar map from its cylindrical spatial position, as follows:

$$r_d = r_i\left(\frac{2+\kappa\left(\frac{d}{r_{cyl}}\right)}{2-\kappa\left(\frac{d}{r_{cyl}}\right)}\right). \quad (35)$$

When a constant r_i term is added to Equation 33, both it and Equation 35 establish a mapping function from the center of the image outward. Equations 33 (with a constant r_i of 0.13738 in added) and 35 were both evaluated for d/r_{cyl} ranging from 0.0 to 0.95, and are plotted for comparison in Figure 10 (in which the dashed line represents the modeled PAL, and the solid line represents constant aspect ratio polar mapping). The two curves agree to within one percent.

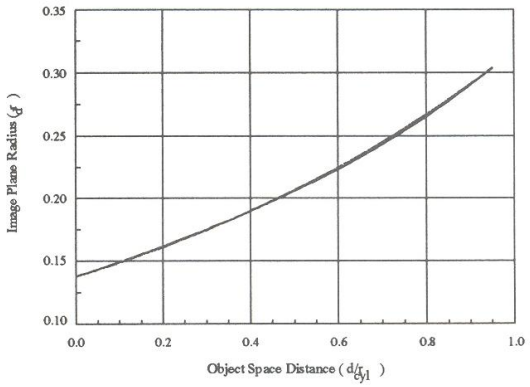

Fig. 10 Image plane radius versus object space distance.

7 CONCLUSION

In conclusion, an analytical model was developed which predicts that the panoramic annular lens produces a constant aspect ratio polar mapping. The model was verified by comparing results with an actual photograph taken through the PAL and with the results obtained using a ray tracing method. This characterization is important; it not only facilitates optical inspection and measurement through a PAL but allows the PAL to be compared with other lenses. These comparisons will be the subject of a subsequent paper.

8 ACKNOWLEDGEMENTS

The authors would like to acknowledge the support provided by NASA's Marshall Space Flight Center, Marquette University and the University of Alabama in Huntsville. Lenses were provided to the project by Optechnology, Inc., Gurley, AL.

9 REFERENCES

1. Mangin, F., *French Patent* No. 125.374; 1878.
2. Bergquist, E.A., *U.S. Patent* No. 3,984,178; 1976.
3. Rees, D. W., *U.S. Patent* No. 3,505,465; 1970.
4. Greguss, P., *U.S. Patent* No. 4,566,763; 1984.
5. Greguss, P., "The Tube Peeper: A New Concept in Endoscopy," *Optics and Laser Technology*, Vol. 17, 1985, pp. 41-45.
6. Gilbert, J.A., Matthys, D.R., Lehner, D.L., Hendren, C.M., "Panoramic Imaging Systems for Nondestructive Evaluation," *Proceedings of the Third Conference on Nondestructive Evaluation for Aerospace Requirements*, Huntsville, Alabama, June 4-6, 1991, pp. 304-310.
7. Gilbert, J.A., Fair, S.B., "Panoramic Endoscopy," *Proceedings of SPIE's Symposium on Optics, Electro-Optics, and Laser Applications in Science & Engineering*, Los Angeles, California, January 19-24, 1992.
8. Gilbert, J.A., Greguss, P., Lehner, D.L., Lindner, J.L., "Radial Profilometry," *Proceedings of the Joint BSSM/SEM International Conference on Advanced Strain Measurement Techniques*, London, England, August 24-27, 1987, Whittles Publishing, pp. 97-107.
9. Greguss, P., Matthys, D.R., Gilbert, J.A., Lehner, D.L., Kransteuber, A.S., "Cavity Inspection Using Radial Metrology," *Proceedings of the Nondestructive Evaluation for Aerospace Requirements Conference*, Huntsville, Alabama, August 22-24, 1989.
10. Gilbert, J.A., Matthys, D.R., Greguss, P., "Optical Measurements Through Panoramic Imaging Systems," *Proceedings of the 1990 International Conference on Hologram Interferometry & Speckle Metrology*, Baltimore, Maryland, November 4-7, 1990, pp. 164-171.
11. Beshears, R.D., Gilbert, J.A., Matthys, D.R., "Nondestructive Examination of Rocket Motor Components," *Proceedings of the 1992 Conference on Advanced Earth-to-Orbit Propulsion Technology*, Huntsville, Alabama, May 19-21, 1992.
12. Gilbert, J.A., Matthys, D.R., Hendren, C.M., "Displacement analysis of the interior walls of a pipe using panoramic holo-interferometry," *Proceedings of SPIE's 1991 International Symposium on Optical & Optoelectronic Applied Science & Engineering*, San Diego, California, July 21-26, 1991, pp. 128-134.
13. Matthys, D.R., Gilbert, J.A., Puliparambil, J., "Panoramic holointerferometry," to be published in *Experimental Mechanics*, 1995.
14. Lindner, J.L., Gilbert, J.A., "Modal analysis using time-average panoramic holo-interferometry," to be published in the *International Journal of Analytical and Experimental Modal Analysis*, 1995.
15. Gilbert, J.A., Greguss, P., Matthys, D.R., Lehner, D.L., "Recent Developments in Radial Metrology: A Computer-Based Optical Method for Profiling Cavities," *Proceedings of Optika '88, Third International Symposium of Modern Optics*, Vol. II, Budapest, Hungary, September 13-16, 1988, pp. 413-418.
16. Matthys, D.R., Greguss, P., Gilbert, J.A., Lehner, D.L., Kransteuber, A.S., "Radial Metrology with a Panoramic Annular Lens," *Proceedings of SPIE's 33rd Annual International Symposium on Optical & Optoelectronic Applied Science & Engineering*, San Diego, California, August 6-11, 1989.
17. Matthys, D.R., Gilbert, J.A., Greguss, P., "Endoscopic Measurement Using Radial Metrology with Digital Correlation," *Optical Engineering*, 30(10): 1455-1460 (1991).
18. Gilbert, J.A., Matthys, D.R., Lehner, D.L., "Moire measurements using a panoramic annular lens," *Proceedings of SPIE's 1991 International Symposium on Optical & Optoelectronic Applied Science & Engineering*, San Diego, California, July 21-26, 1991, pp. 202-209.
19. Gilbert, J.A., Fair, S.B., Caldwell, S.E., Gronner, S.J., "A Hemispherical Imaging and Tracking (HIT) System," *Proceedings of AIAA's Endoscopic Kinetic Energy Weapon Technology Conference*, Huntsville, Alabama, May 19-21, 1992.
20. Gilbert, J.A., Bankston, C.D., "A "PARC" System for Terminal Docking," *Proceedings of the U.S. Automated Rendezvous and Capture Capabilities Review,* Office of Space Flight, NASA Headquarters, Williamsburg, Virginia, November 19-21, 1991, pp. 33-33II.
21. Bankston, C.D., Gilbert, J.A., "A satellite-based imaging system for attitude determination and remote sensing," *Proceedings of the SEM Spring Conference and Exhibits*, Grand Rapids, Michigan, June 12-15, 1995.
22. Greguss, P., Gilbert, J.A., Matthys, D.R., Lehner, D.L., "Developments in Radial Metrology," *Proceedings of SPIE International Symposium on Optical Engineering and Industrial Sensing for Advanced Manufacturing Technologies*, Vol. 954, Dearborn, Michigan, June 25-30, 1988, pp. 392-398.
23. Matthys, D.R., Gilbert, J.A., Puliparambil, J., "Endoscopic Inspection Using a Panoramic Annular Lens," *Proceedings of SPIE's 1991 International Symposium on Optical & Optoelectronic Applied Science & Engineering*, San Diego, California, July 21-26, 1991, pp. 736-742.
24. Gilbert, J.A., Matthys, D.R., Hendren, C.M., "Endoscopic Inspection and Measurement," *Proceedings of SPIE's Symposium on Image and Signal Processing*, San Diego, California, July 19-24, 1992.
25. Lehner, D.L., "Radial Metrology," *Ph.D. Thesis*, University of Alabama in Huntsville, Huntsville, AL, 1994.
26. Steadham, M.A., "Measurement of Spacecraft Attitude Via the Panoramic Annular Lens Attitude Determination System (PALADS)," *M.S. Thesis*, University of Alabama in Huntsville, Huntsville, AL, 1994.
27. Richter, A.G., "Characterization of a Panoramic Annular Lens," *M.S. Thesis*, Marquette University, Milwaukee, WI, 1992.